RSC Advances

PAPER

View Article Online
View Journal | View Issue

Check for updates

Cite this: *RSC Adv.*, 2022, **12**, 21503

Development of nitrile rubber/eucommia ulmoides gum composites for controllable dynamic damping and sound absorption performance

Lin Su,[a] Qi Wang,[b] Ping Xiang,[a] Dexian Yin, *[b] Xiaodong Ding,[a] Li Liu[b] and Xiuying Zhao*[b]

Aiming at enhancing the damping and sound absorption performances of nitrile rubber (NBR) incorporated Eucommia ulmoides gum (EUG), a series of NBR/EUG composites were successfully fabricated using an open mixing mill. The co-vulcanization behaviors, fracture surface morphology observations, mechanical and thermal properties and damping and sound absorption performances of NBR/EUG composites were investigated systematically. It was shown that the crystalline area and the amorphous area in NBR/EUG composites displayed a sea-island phase distribution and most of the EUG crystals were β-form crystals. Compared to that of neat NBR, the tensile strength and storage modulus of NBR/EUG composites increased dramatically with the increasing EUG content, owing to the gradually increasing number of crystals in the NBR/EUG composites. In addition, the incorporation of EUG into the NBR matrix distinctly improved the sound absorption performance of NBR/EUG composites. This work is expected to provide a new insight into the fabrication of other composite materials with controllable damping and sound absorption properties.

Received 10th June 2022
Accepted 19th July 2022

DOI: 10.1039/d2ra03597a

rsc.li/rsc-advances

Open Access Article. Published on 02 August 2022. Downloaded on 7/8/2025 12:13:42 PM.
This article is licensed under a Creative Commons Attribution-NonCommercial 3.0 Unported Licence.

1 Introduction

As one of the main types of environmental pollution, noise pollution significantly endangers human health, accelerates mechanical breakdown and affects ecological systems.[1,2] Specifically speaking, noise pollution not only damages the hearing and influences the sleeping quality of people but also affects the precision and working life of machines.[3] Considering the components of turbine machinery such as large compressors and air fans, the problem continues to get worse and needs to be solved urgently. With the development of materials in recent decades, damping materials have become a growing research hotspot owing to the advantages of noise and vibration reduction.[4,5] Among them, rubber with its unique viscoelastic property exhibits obvious superiority in the aspect of vibration damping applications because rubber could consume noise and vibration energy as heat energy, which has been applied extensively in transportation equipment, building, aerospace and so on.[6,7]

Acrylonitrile-butadiene rubber, commonly called nitrile rubber (NBR), plays an important role in synthesized rubber fields and has gained considerable attention in damping application fields on account of its remarkable oil and water resistance.[8–10] However, under the fast development of industry and society, the damping performance of NBR is not satisfactory, especially under extreme operating conditions.

Eucommia ulmoides gum (EUG), existing in barks, leaves and fruit coatings of Eucommia ulmoides trees, is a natural polymer with double characteristics of plastic and rubber.[11] The chemical structure of EUG is *trans*-1, 4-polyisoprene and the chemical structure of natural rubber (NR) is *cis*-1, 4-polyisoprene, which displayed isomers of each other.[12] Compared with NR, EUG is inclined to crystallization owing to the more regular molecular structure.[13] Two crystal forms exist in EUG matrix including α-crystals and β-crystals with different melting points, and EUG owns outstanding damping properties on account of its crystal melting transition.[14] In the meantime, EUG possesses a higher modulus than traditional rubber because of the existing crystals, which could resist deformation under extreme operating conditions. A hopeful strategy for obtaining diversified new-type damping elastomers with excellent comprehensive properties could be implemented *via* blending EUG with other synthetic rubbers.

Herein, a feasible method to fabricate NBR/EUG composites with adjustable modulus and excellent damping properties was proposed by changing the content of EUG. The effects of mixing technology and vulcanization system on the co-vulcanization of NBR and EUG were studied, and different proportions of NBR/EUG composites were prepared by using open mixing mill. The fracture surface morphology, thermal performance, mechanical property as well as damping and sound absorption behaviors of

[a]*Systems Engineering Research Institute, Beijing, 100094, China*
[b]*Key Laboratory of Beijing City on Preparation and Processing of Novel Polymer Materials, Beijing University of Chemical Technology, Beijing, 100029, China. E-mail: yindx96@163.com; zhaoxy@mail.buct.edu.cn*

© 2022 The Author(s). Published by the Royal Society of Chemistry

Open Access Article. Published on 02 August 2022. Downloaded on 7/8/2025 12:13:42 PM. This article is licensed under a Creative Commons Attribution-NonCommercial 3.0 Unported Licence.

various NBR/EUG composites were systematically investigated, and the correlation between these properties and the special microstructure has been researched in this work. This work may provide a promising strategy for developing other composite materials with outstanding damping and sound absorption properties.

2 Experimental

2.1 Materials

NBR (N220S) with a content of 42% acrylonitrile was supplied by JSR Corporation, Japan. EUG with the number-average molecular weights of 122 915 and polydispersity index of 2.073 was bought from China Ankang Hanyin Hua Ye Plant Pharmaceutical Co. Ltd. Other experimental materials were bought from common manufacturers in the rubber industry of China.

2.2 Preparation of various NBR/EUG composites

The preparation steps of various NBR/EUG composites were as follows and the corresponding experimental photos were exhibited in Fig. 1. Step 1: EUG was plasticized on a hot open mixing mill for 1 min at 60 °C (Fig. 1a). Step 2: NBR was added into EUG matrix (Fig. 1b). Step 3: S, ZnO, stearic acid (SA) and accelerant were ordinal added for uniform mixing (Fig. 1c). Step 4: the roller spacing was adjusted to the minimum, and triangle bag shape was made six times for better mixing (Fig. 1d). Then, the roller spacing was adjusted to 2 mm and NBR/EUG composites were subsequently fabricated.

About 5.0 g of NBR/EUG composites were put into a vulcanizing instrument at a vulcanization temperature of 150 °C and the process positive vulcanization time T_{90} of NBR/EUG composites was obtained. Then various NBR/EUG composites were fabricated *via* an electric plate vulcanizing machine for T_{90} + 2 min at 25 MPa.

2.3 Characterizations

2.3.1. Co-vulcanization. The vulcanization characteristics of NBR/EUG composites were confirmed by a MR-C3 vulkameter (Beijing Ruida Yu Chen Instrument Co., Ltd., China). About 5 g composites were cut and padded with thin cellophane on both sides. The temperature was set to 150 °C with a holding time of 30 min.

2.3.2. Atomic force microscopy (AFM). The micromorphology of NBR/EUG composites was observed *via* AFM (Multi Mode 8, Bruker, Germany) with Peak Force Quantitative Nano Mechanics (QNM) mode. Before observations, the composites were polished by a cryo-ultramicrotome (Leica EM UC7, Germany).

2.3.3. Scanning electron microscopy (SEM). Further micromorphology observation of NBR/EUG composites was examined by SEM (S-4800, Hitachi, Japan). Before observation, NBR/EUG composites were freeze-fractured under liquid nitrogen and were sputter-coated with Au.

2.3.4. Mechanical performances. The mechanical performance of NBR/EUG composites was examined by CMT4104 tensile tester (SANS Ltd., Shenzhen, China) based on ASTM Standard D638. The dumbbell-shaped NBR/EUG composites (6 mm × 2 mm) were stretched at 500 mm min^{-1} and all composites were repeated three times to take the average value.

2.3.5. Dynamic mechanical thermal analyses (DMTA). DMTA of NBR/EUG composites was carried out on a dynamic mechanical thermal analyzer (DMTA, VA-3000, Metravib, France) with a shape of rectangle (6 mm × 2 mm × 20 mm). The curves of composites were measured at the temperature range from −80 °C to 100 °C with a heating rate of 10 °C min^{-1}, 0.3% tensile strain, and a frequency of 10 Hz.

2.3.6. Differential scanning calorimetry (DSC). DSC analyses of NBR/EUG composites were performed on a thermal analyzer (STARe system, Mettler Toledo, Switzerland) under nitrogen atmosphere. The composites were first quickly heated from room temperature to 100 °C, then held for 5 min and cooled to −100 °C, and heated back to 100 °C. The rate of temperature increasing and decreasing was set as 10 °C min^{-1}.

2.3.7. X-ray diffractometer (XRD). XRD analysis was conducted on NBR/EUG composites with an XRD instrument (D/max-2500, Rigaku, Japan). The composites were scanned at a scattering range of 5–30° and a scanning rate of 3° min^{-1} using Cu Kα. The crystallinity index (χ_c) of NBR/EUG composites was calculated *via* eqn (1) and the crystallite size was calculated by Scherrer's formula *via* eqn (2).

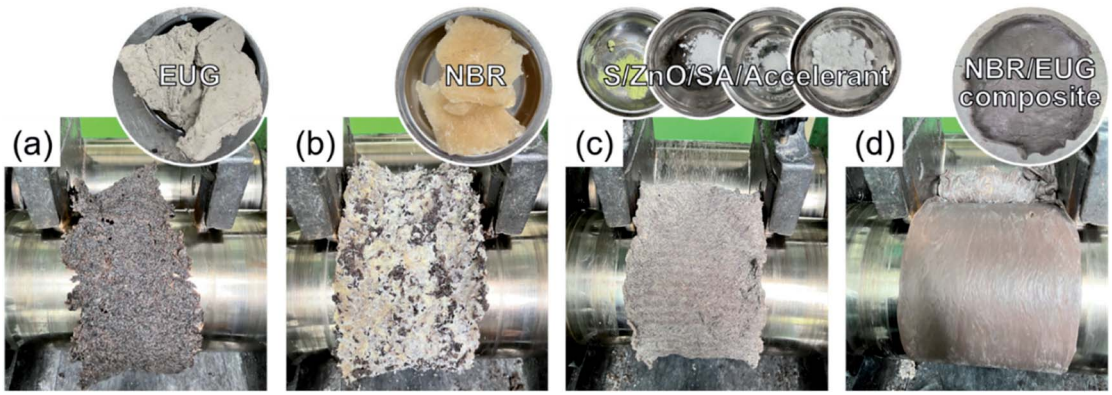

Fig. 1 The fabrication process of various NBR/EUG composites by using open mixing mill.

© 2022 The Author(s). Published by the Royal Society of Chemistry

Open Access Article. Published on 02 August 2022. Downloaded on 7/8/2025 12:13:42 PM.
This article is licensed under a Creative Commons Attribution-NonCommercial 3.0 Unported Licence.

$$\chi_c = \frac{I_c}{I_c + I_a} \times 100\% \quad (1)$$

where I_c is the peak intensity attributed to the crystalline area, I_a is the peak intensity of the amorphous fraction.

$$\text{Crystallite} = \frac{K\lambda}{\beta \cos\theta} \quad (2)$$

in which K is the shape factor with a value of 0.9, λ is the wavelength of X-ray used ($\lambda = 0.15406$ nm), β is the full width half maximum and θ is the diffraction angle.

2.3.8. Sound absorption coefficients (SAC). The SAC of NBR/EUG composites were measured *via* an acoustic tube measuring system (height = 50 mm, diameter = 120 mm) under the frequency bands of 3–8 kHz and pressure bands of 1–2.5 MPa at a water temperature of 15 °C, room temperature of 20 °C and humidity of 52% RH.

3 Results and discussion

3.1 Co-vulcanization behavior of NBR and EUG

Vulcanization of rubber plays a very important role in the comprehensive properties of rubber. Generally speaking, different kinds of rubber display thermodynamics incompatible, and co-vulcanization process is needed to achieve good mechanical performance. NBR is a polar rubber with polar side groups, and EUG exhibits different properties according to different degrees of vulcanization, thus it is very important to select the appropriate formula and process conditions.

In this work, five kinds of accelerators commonly used in NBR and EUG processing were selected and showed in Fig. 2. Accelerator TMTD as a type of thiuram accelerator is widely used in NBR vulcanization, because it could give rubber outstanding permanent deformation properties of compression. But the coke safety of thiuram accelerators is froward and the spray frost effect is relatively obvious. Accelerators NS and CZ are kinds of sulfenamide accelerators, it owns the advantages of high activation performance, fast reaction rate and scorch safety. The drawback is that the single use of sulfenamide type accelerators could lead to low crosslinking density of rubber. Accelerator DTDM is also a sulphur donor with the advantages of safe operation, no spray frost and invariant color. However, the vulcanization rate is relatively slow when it used alone. Accelerator D as a part of guanidine accelerator is often utilized as accessory ingredient.

There were two considerations when designing NBR/EUG vulcanization systems. One was that good compatibility of NBR and EUG was required to optimize the overall mechanical properties. The other was that a majority of vulcanizing agents should be distributed in NBR matrix to obtain the optimum mechanical properties of NBR under the vulcanization process, in the meantime, the vulcanization process would not destroy the main crystalline region in EUG matrix. Based on the above analysises, five different vulcanization formulas were designed in this work, which were shown in Table 1. The mechanical properties of NBR/EUG composites with different formulas were displayed in Fig. 3 and Table 2.

It could be found in Fig. 3 and Table 2 that compared to other formulas, formula 2 displayed the highest tensile strength and hardness, in which the accelerators TMTD and D were utilized in this formula. Accelerator TMTD consists of two active groups and two accelerator groups (Fig. 2), in which the active sulfur atoms are precipitated to participate in the vulcanization reaction during the vulcanization process. As a kind of acid accelerator, the distribution coefficient of TMTD in NBR is higher than that of EUG. Accelerator D with relatively slow vulcanizing speed and high operation safety could be dissolved in both NBR and EUG matrix. The combination of accelerator TMTD and D could effectively vulcanize NBR while retaining part of the crystalline region of EUG, so formula 2 was chosen as the final formula to conduct the follow-up experiments. Based on formula 2, various NBR/EUG composites with NBR/EUG ratios of 100/0, 95/5, 90/10, 85/15, 80/20, 70/30, 60/40, 50/50, and 0/100 were fabricated on the hot roll mixer.

3.2 Microstructure observations

The quantitative nanomechanical technique of atomic force microscopy (AFM-QNM), a mature technique for the research of polymer morphology at the sub-nanometer spatial resolution, was utilized to investigate the influence of EUG on the morphology of various NBR/EUG composites. Fig. 4 displayed the AFM images of NBR/EUG composites at different ratios of 95/5, 90/10, 80/20, 70/30, 60/40, and 50/50. The light regions represent the high modulus area and the dark regions represent the low modulus area, and the phase distribution of NBR/EUG

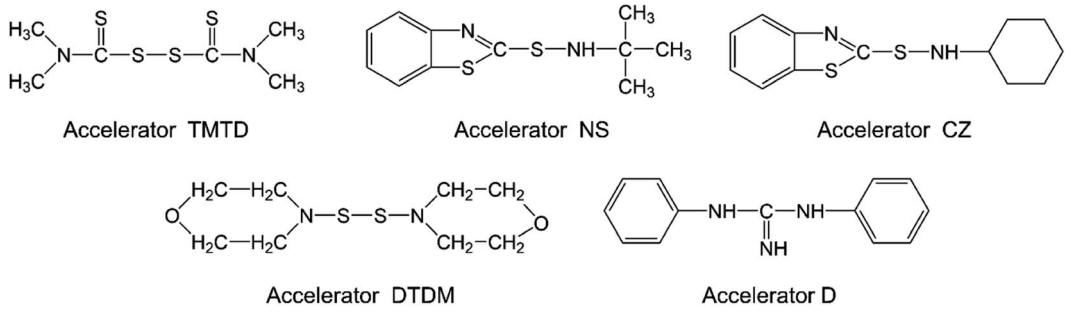

Fig. 2 Chemical structure of different accelerators.

Open Access Article. Published on 02 August 2022. Downloaded on 7/8/2025 12:13:42 PM.
This article is licensed under a Creative Commons Attribution-NonCommercial 3.0 Unported Licence.

Table 1 Formulas for NBR/EUG co-vulcanization research[a]

Component (phr)	Formula 1	Formula 2	Formula 3	Formula 4	Formula 5
NBR	80	80	80	80	80
EUG	20	20	20	20	20
ZnO	5	5	5	5	5
SA	2	1	2	2	2
Accelerator TMTD	0	0.2	0.2	0	0
Accelerator NS	0	0	0.8	1.2	0
Accelerator CZ	0	0	0	0	0.8
Accelerator DTDM	3	0	0	0	0
Accelerator D	1	1	0	0	0
S	2	2	2.5	2.5	2.5

[a] Notes: TMTD (tetramethyl thiuram disulfide); NS (*N*-tertbutyl-2-benzothiazole sulfonamide); CZ (*N*-cyclohexyl-2-benzothiazole sulfonamide); DTDM (4,4′-dithio-dimorpholine); D (diphenyl guanidine).

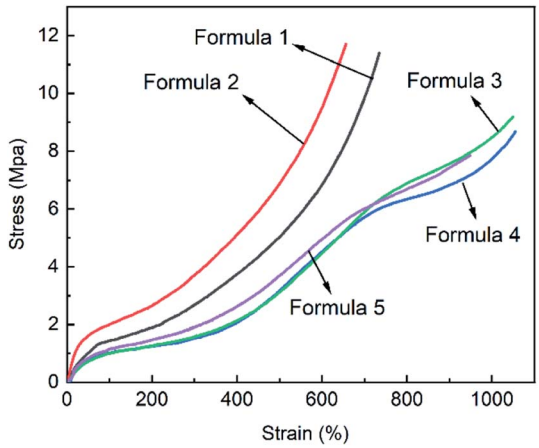

Fig. 3 Stress–strain curves of NBR/EUG composites with different formulas.

composites could be explored through the color distribution. It could be found in Fig. 4 that the light regions represented the EUG phase (with an ellipsoid shape) and the dark regions represented the NBR phase, which showed a "sea-island" phase distribution. As displayed in Fig. 4(a–c), when the amount of EUG was small (lower than 30%), the distribution of EUG phase was uniform and no large aggregation phase formed in NBR/EUG composites. It illustrated that during the processing process, a small quantity of EUG could be uniformly dispersed in the NBR matrix *via* strong mechanical shear force.[15] The EUG phase could reinforce NBR matrix on account of the interface interaction between EUG and NBR as well as the crosslinking network of sulfur. As shown in Fig. 4(d–f), the EUG phase with high Young's modulus aggregated into a larger island phase in the NBR phase when the amount of EUG was high (30% or above) in NBR matrix. Owing to the crystallization effect of EUG, a large amount of EUG in NBR matrix was likely to cause stress concentration, leading to the formation of small cracks at the two-phase interface and the reduction of mechanical properties of NBR/EUG composites.[16,17]

The morphologies of polymeric composites strongly influence the properties of composites owing to the interfacial interaction of the two-phase interfaces. Thus, the fractured surface morphologies of various NBR/EUG composites were further investigated by SEM and the relevant photographs were shown in Fig. 5. As displayed in Fig. 5a, the NBR/EUG (95/5) composite presented a relatively smooth surface and a bit of EUG phase could be observed, which was uniformly distributed throughout NBR matrix. However, the size of the spherical EUG phase was visibly increased with the increase of EUG content (Fig. 5(b and c)). Especially, when the addition of EUG was more than 20%, two distinct phases could be found on the surfaces of NBR/EUG composites and the SEM photographs exhibited typical sea-island structures, in which elliptical EUG phase dispersed in continuous NBR matrix. The observations demonstrated that a small amount of EUG content could be uniformly dispersed in NBR matrix. However, with an increasing amount of EUG in NBR/EUG composites, the two-phase interface between NBR and EUG presented a weak interfacial adhesion and poor compatibility because of the

Table 2 Mechanical properties of NBR/EUG composites with different formulas

Mechanical properties	Formula 1	Formula 2	Formula 3	Formula 4	Formula 5
Tensile strength (MPa)	11.9 ± 0.3	12.3 ± 0.4	9.3 ± 0.3	8.8 ± 0.1	8.2 ± 0.2
Elongation at break (%)	753 ± 13	675 ± 8	1114 ± 12	1035 ± 15	1019 ± 11
100% elongation stress (MPa)	1.6 ± 0.3	2.0 ± 0.1	1.0 ± 0.2	1.0 ± 0.1	1.2 ± 0.1
300% elongation stress (MPa)	2.7 ± 0.2	3.6 ± 0.3	1.5 ± 0.1	1.6 ± 0.1	2.0 ± 0.1
Tensile permanent deformation (%)	20 ± 3	19 ± 0	62 ± 4	51 ± 3	55 ± 1
Hardness (Shore A)	59.8 ± 0.2	63.2 ± 0.3	48.9 ± 0.1	49.8 ± 0.4	51.3 ± 0.2

© 2022 The Author(s). Published by the Royal Society of Chemistry

Open Access Article. Published on 02 August 2022. Downloaded on 7/8/2025 12:13:42 PM.
This article is licensed under a Creative Commons Attribution-NonCommercial 3.0 Unported Licence.

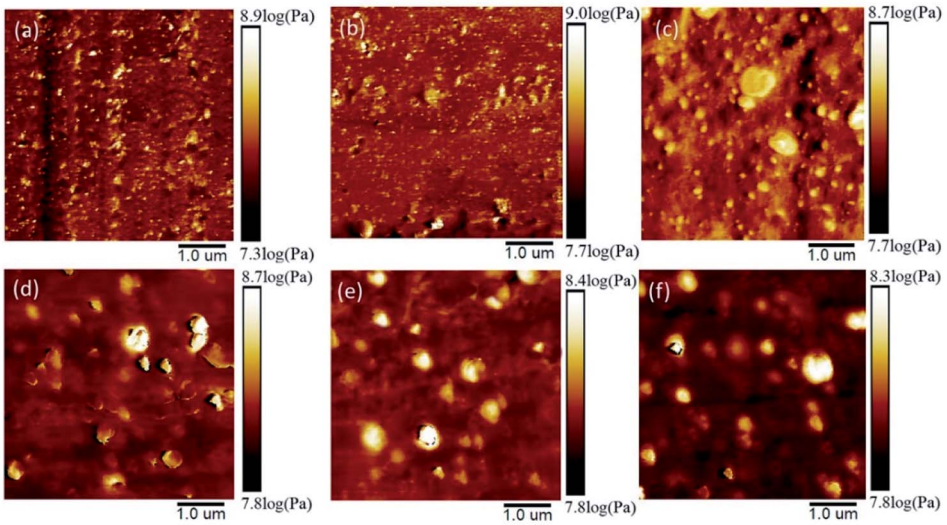

Fig. 4 AFM images of various NBR/EUG composites: (a) NBR/EUG = 95/5; (b) NBR/EUG = 90/10; (c) NBR/EUG = 80/20; (d) NBR/EUG = 70/30; (e) NBR/EUG = 60/40; (f) NBR/EUG = 50/50.

crystallization of EUG, resulting in the appearance of stress concentration phenomenon and possibly poor mechanical property of NBR/EUG composites.[15]

3.3 Mechanical properties

The mechanical properties of NBR/EUG composites including Shore hardness, tensile strength, elongation at break, stress at definite elongation (100% and 300%), tensile permanent deformation and stress–strain curves were investigated and exhibited in Fig. 6 and Table 3. In Fig. 6, the Shore hardness of neat NBR was 53A. The addition of EUG to NBR led to considerable enhancement in the Shore hardness of various NBR/EUG composites, which increased from 53A to 83A. The reason was that the existed crystals of EUG in NBR matrix displayed a relatively high Shore hardness, which observably enhanced the Shore hardness of NBR/EUG composites.

As shown in Fig. 6 and Table 3, the tensile strength and elongation at break of NBR/EUG composites improved from 4.4 to 13.0 MPa and from 409% to 689%, respectively, with increasing EUG content from 0% to 10%. With EUG content in NBR matrix of more than 10%, the tensile strength and elongation at break of NBR/EUG composites decreased, which were still higher than those of NBR. It was because a small amount of EUG content dispersing in NBR matrix could be acted as physical intersection points, leading to the increase of the mechanical properties of NBR/EUG composites.[18,19] Nevertheless, a large amount of EUG caused the formation of large size crystals in NBR matrix, leading to stress concentration and formation of small cracks at the two-phase interface as well as the reduction of mechanical properties of NBR/EUG composites, which could be observed in AFM and SEM photographs (in Fig. 4 and 5). Hence, the tensile strength and elongation at

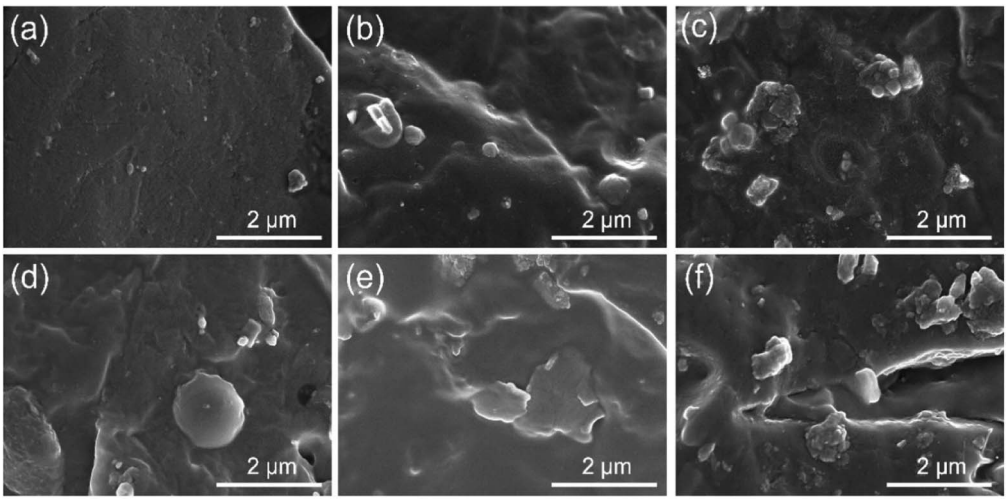

Fig. 5 SEM images of various NBR/EUG composites: (a) NBR/EUG = 95/5; (b) NBR/EUG = 90/10; (c) NBR/EUG = 80/20; (d) NBR/EUG = 70/30; (e) NBR/EUG = 60/40; (f) NBR/EUG = 50/50.

Open Access Article. Published on 02 August 2022. Downloaded on 7/8/2025 12:13:42 PM.
This article is licensed under a Creative Commons Attribution-NonCommercial 3.0 Unported Licence.

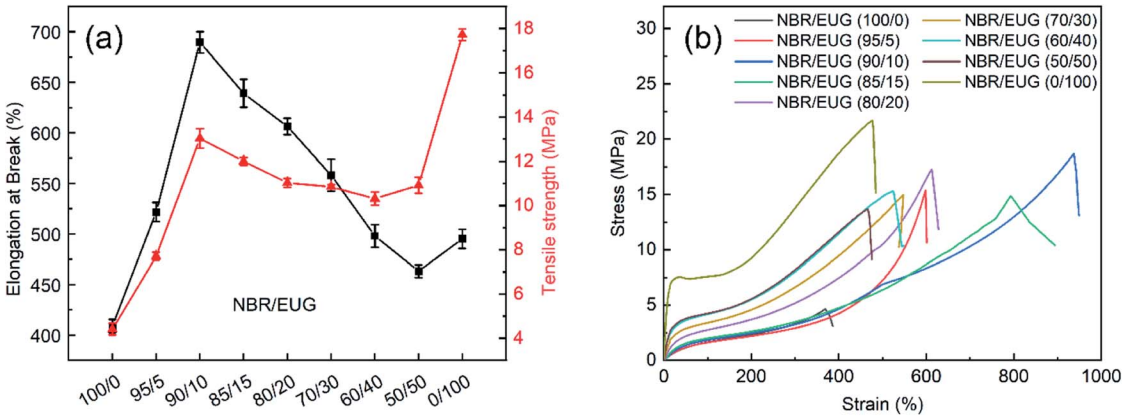

Fig. 6 Mechanical properties of various NBR/EUG composites: (a) elongation at break and tensile strength; (b) stress–strain curves.

break of NBR/EUG composites first increased to their optimal value and then decreased gradually with EUG content increased from 0% to 50%, and the NBR/EUG (90/10) composite displayed maximum tensile strength and elongation at break values among these NBR/EUG composites. Moreover, owing to the particular rubber-plastic character of EUG, various NBR/EUG composites changed from elastic rubber materials to tough plastic materials (in Fig. 6b) and the stress at definite elongation (100% and 300%) increased gradually (in Table 3) with the increasing content of EUG in NBR matrix.

3.4 Damping properties

DMA was utilized to investigate the dynamic response of various NBR/EUG composites and Fig. 7 displayed the temperature dependence of loss factor (tan δ) and storage modulus (E') for the composites.

Tan δ curve, the ratio of loss modulus/E', was regarded as a measurement of material damping ability (*i.e.*, dissipation of vibration energy) and the glass transition temperature (T_g) of materials could be obtained by the maximum value of tan δ curves. As exhibited in Fig. 7a, the tan δ of NBR/EUG composites displayed a maximum value at the temperature of around 0 °C, and another peak could be seen at around −50 °C because of the glass transition behavior of EUG.[20] With the increasing content of EUG from 0% to 50%, the T_g of NBR/EUG composites decreased gradually and shifted to a lower temperature, in the meantime, the tan δ curves of various NBR/EUG composites changed from a single peak to double peaks (in red frame of Fig. 7a), especially in the tan δ curves of NBR/EUG (60/40) composite, NBR/EUG (50/50) composite and NBR/EUG (0/100) composite. The appearance of double peak phenomena suggested that the compatibility of NBR and EUG phases in NBR/EUG composites decreased with the increase of EUG content.[19,21]

The E' of various NBR/EUG composites were shown in Fig. 7b. As could be seen from Fig. 7b, the E' of all NBR/EUG composites underwent two transformations, corresponding to the glass transition of NBR and the crystal melting of EUG respectively. Increasing the content of EUG, a successive increase of E' values could be observed in various NBR/EUG composites between −20 °C to 50 °C. The reason was that EUG could crystallize in this temperature range, which significantly improved the E' of NBR/EUG composites.[15,18,22] With further increasing the temperature (above 50 °C), EUG crystals reached their melting temperature and displayed amorphous conditions, which led to a sharp decrease of E' in NBR/EUG composites. The results indicated that the E' of NBR/EUG composites could be effectively regulated by changing the content of EUG in the composites.

3.5 Crystallization and melting properties

XRD was carried out to evaluate the crystallization performances of various NBR/EUG composites with different contents of EUG, and Fig. 8a exhibited the relevant XRD curves. It was found in Fig. 8a that no diffraction peak appeared in NBR/EUG (100/0) composite owing to the noncrystalline structure of pure

Table 3 Mechanical properties of various NBR/EUG composites

	NBR/EUG								
Mechanical properties	100/0	95/5	90/10	85/15	80/20	70/30	60/40	50/50	0/100
Tensile strength (MPa)	4.4 ± 0.3	7.7 ± 0.2	13.0 ± 0.4	12.0 ± 0.2	11.0 ± 0.2	10.8 ± 0.1	10.3 ± 0.3	10.9 ± 0.4	17.7 ± 0.3
Elongation at break (%)	409 ± 7	522 ± 10	689 ± 11	639 ± 14	606 ± 8	558 ± 16	498 ± 11	463 ± 6	495 ± 10
100% elongation stress (MPa)	1.2 ± 0.1	1.3 ± 0.2	1.5 ± 0.2	1.7 ± 0.1	2.2 ± 0.1	2.7 ± 0.0	3.1 ± 0.1	3.5 ± 0.1	5.8 ± 0.1
300% elongation stress (MPa)	2.5 ± 0.1	2.4 ± 0.1	2.6 ± 0.1	3.0 ± 0.3	4.2 ± 0.3	5.0 ± 0.1	5.9 ± 0.1	6.7 ± 0.3	10.7 ± 0.2
Tensile permanent deformation (%)	0 ± 0	0 ± 0	4 ± 1	12 ± 0	12 ± 1	28 ± 1	28 ± 0	40 ± 0	88 ± 1
Hardness (Shore A)	53 ± 1	54 ± 2	57 ± 1	59 ± 2	62 ± 0	70 ± 0	75 ± 2	79 ± 1	83 ± 2

© 2022 The Author(s). Published by the Royal Society of Chemistry

Open Access Article. Published on 02 August 2022. Downloaded on 7/8/2025 12:13:42 PM.
This article is licensed under a Creative Commons Attribution-NonCommercial 3.0 Unported Licence.

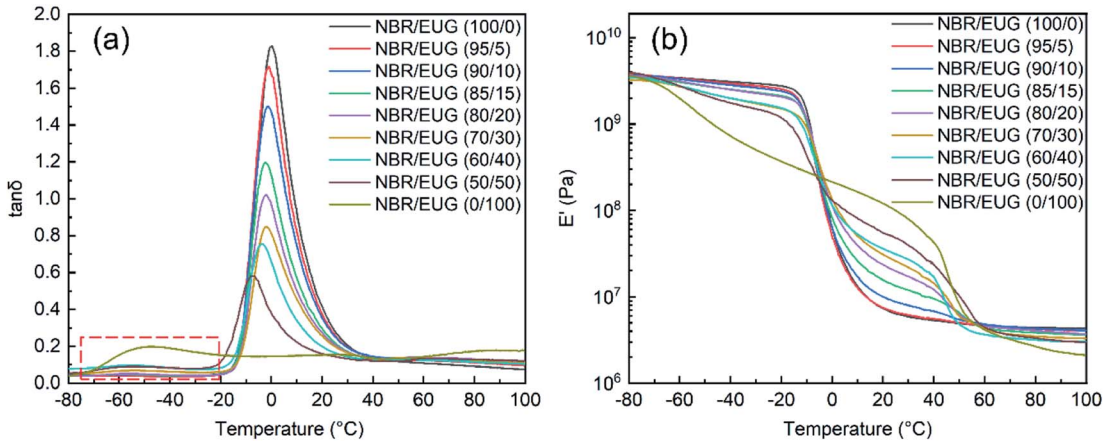

Fig. 7 Tan δ and E' of various NBR/EUG composites.

NBR. When a small amount of EUG (10 phr) incorporated in NBR, two diffraction peaks started to appear near 18.7° and 22.7°, as displayed in the XRD curve of NBR/EUG (90/10) composite. With the content of EUG increasing from 10 to 100 phr, another diffraction peak at around 26.9° was observed in the XRD curve of NBR/EUG (70/30) composite and the intensity of the aforementioned three diffraction peaks gradually increased, which was pretty obvious in the XRD curve of NBR/EUG (0/100) composite. The appearance of these diffraction peaks was attributed to the existing crystals of EUG (containing α- and β-form crystalline structures) in NBR matrix, in which the peak of the α-form crystalline structure of EUG was at 22.7° and the peaks of the β-form crystalline structure of EUG were at 18.7° and 22.7°.[23,24] Notably, the diffraction peak at 22.7° displayed a low intensity while the diffraction peaks at 18.7° and 22.7° showed a relatively high intensity among all NBR/EUG composites, which indicated that most of the EUG crystals in NBR/EUG composites were β-form crystals.[25,26] Different temperatures facilitated the formation of α and β crystals during the isothermal crystallization of EUG, in which α crystal displayed a thermodynamic stable form and β crystal showed a metastable form. Thus, β crystals were produced easily at a fast cooling rate during the non-isothermal crystallization of EUG.[27]

In addition, the size of the EUG crystals in NBR/EUG composites could be calculated from the XRD data *via* the Scherrer formula. The average crystal size of EUG determined from the diffraction peaks of 18.7°, 22.7° and 26.9° was shown in Table 4, in which the data with a large error calculated by the Scherrer formula was eliminated. As listed in Table 4, all EUG crystal sizes existed in the scope of 1 to 32 nm, indicating that the agglomeration phenomenon of EUG crystals did not occur in NBR/EUG composites. Meanwhile, it could be found in Table 4 that the χ_c of various NBR/EUG composites increased with the increase of EUG content.

To further investigate the crystallization performances of various NBR/EUG composites, DSC was employed and the related DSC graph was given in Fig. 8b. According to the DSC results, the curve of pure NBR showed an obvious glass transition peak at about 14 °C. With the increase of EUG content, the glass transition peak became less obvious until it disappeared (in red frame of Fig. 8b), ascribing to the following two reasons. On one hand, the incorporation of EUG increased the number of crystals in NBR matrix, limiting the movement and

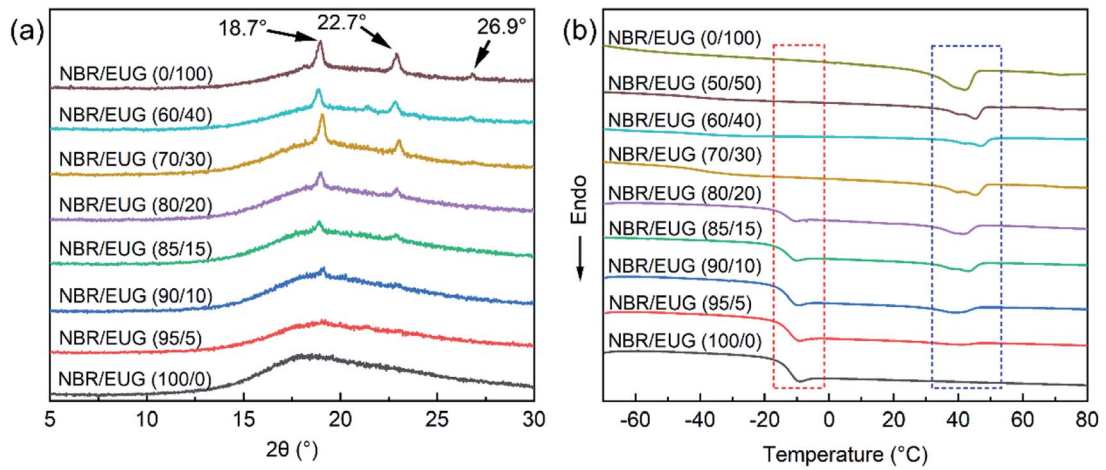

Fig. 8 XRD and DSC curves of various NBR/EUG composites.

Open Access Article. Published on 02 August 2022. Downloaded on 7/8/2025 12:13:42 PM.
This article is licensed under a Creative Commons Attribution-NonCommercial 3.0 Unported Licence.

Table 4 Average crystal size and crystallinity of various NBR/EUG composites

	NBR/EUG								
Crystallization properties	100/0	95/5	90/10	85/15	80/20	70/30	60/40	50/50	0/100
Average crystal size (18.7°) (nm)	—	—	—	8.3	7.0	14.8	23.6	22.4	21.4
Average crystal size (22.7°) (nm)	—	—	—	1.6	2.9	16.5	29.7	20.7	23.9
Average crystal size (26.9°) (nm)	—	—	—	—	—	23.7	31.8	30.0	31.8
χ_c (%)	—	—	—	4.22	4.96	5.93	7.21	7.77	6.62

rearrangement of chain segments during the glass transition region.[28–30] On the other hand, increasing EUG content in NBR/EUG composites signified the reduction of the proportion of NBR content. Moreover, with the increase of EUG content, the melting peak of various NBR/EUG composites appeared gradually and the melting peak area was getting larger and larger (in blue frame of Fig. 8b), indicating the crystallization performances of the fabricated NBR/EUG composites were able to change by adjusting the content of EUG in NBR matrix.[17]

3.6 Sound absorption performances

Effects of EUG content, water pressure and frequency of various NBR/EUG composites on the change of SAC with the frequency of sound wave were exhibited in Fig. 9. It showed that all curves fluctuated within a narrow range owing to the resonant absorption of sound.[31,32] In addition, the SAC data of various NBR/EUG composites fluctuated greatly and the rule of curve variation was not obvious under the water pressure of 1.0 MPa, which might be the instability of the test instrument.

In Fig. 9, the SAC of NBR/EUG composites distinct improved with the increase of frequency, attributing to that high frequency means short wavelength and comparatively weak penetrating power. It also could be seen from Fig. 9 that the SAC of NBR/EUG composites increased with the increasing EUG content from 0% to 20%, which was obviously regular under high-pressure conditions (*e.g.*, 2.0 or 2.5 MPa). The reason should be attributed to two aspects. One is that the incorporated EUG crystals enhanced the modulus of NBR/EUG composites, which increased the propagation speeds of sonic waves and improved the impedance matching between the composites and water.[14,31,33] The other is that the sound impedance of the crystals in NBR/EUG composites mismatched that of water, and thus the incident sound wave reflection happened and reflected many times when it met the crystals.[15] As a result, the propagation path of sound waves was changed and increased, leading to the enhancement of the sound energy dissipation. However, the SAC slightly decreased when EUG content further increased, due to that the excess crystals in

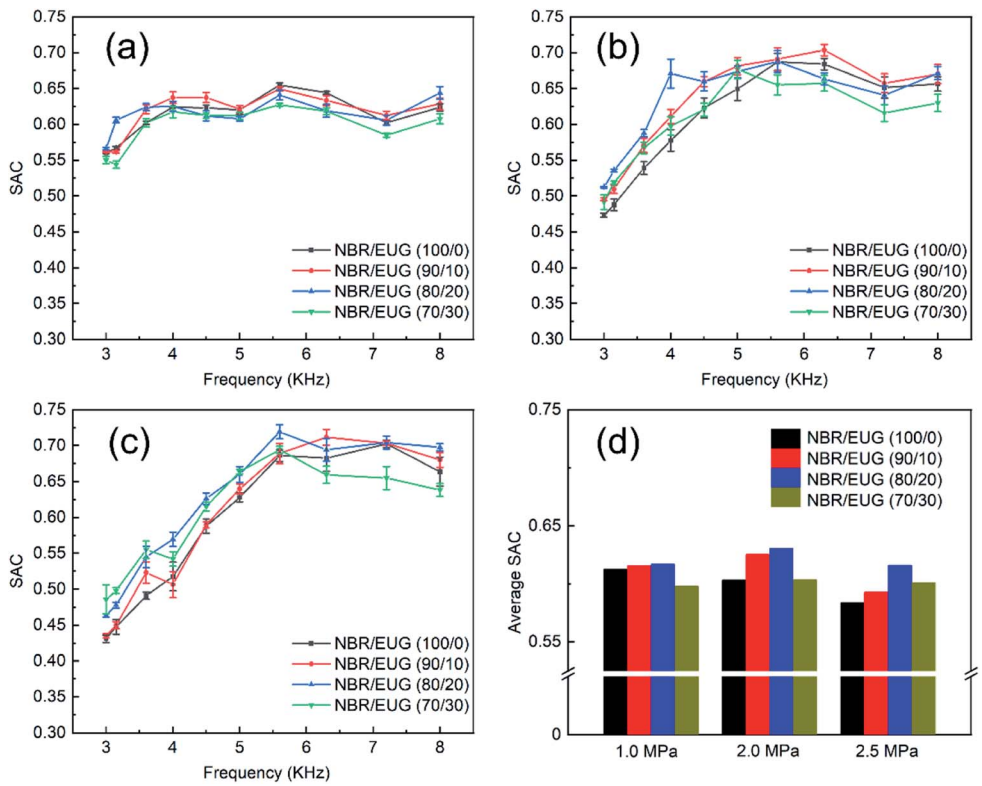

Fig. 9 SAC of various NBR/EUG composites under different pressures ((a) 1.0 MPa; (b) 2.0 MPa; (c) 2.5 MPa) and (d) average SAC.

© 2022 The Author(s). Published by the Royal Society of Chemistry

Open Access Article. Published on 02 August 2022. Downloaded on 7/8/2025 12:13:42 PM.
This article is licensed under a Creative Commons Attribution-NonCommercial 3.0 Unported Licence.

NBR/EUG composites would hinder the movement of molecular chains and thus affect there damping performances as well as the sound energy dissipation.

4 Conclusions

In this paper, various NBR/EUG composites with controllable damping and sound absorption performances were successfully fabricated. AFM and SEM observations stated that various NBR/EUG composites displayed a distinct sea-island phase distribution. XRD and DSC results illustrated that with the increasing of EUG content, the χ_c of various NBR/EUG composites gradually improved and most of the EUG crystals exhibited β-form crystals. Additionally, the tensile strength and E' of NBR/EUG composites increased dramatically with the increasing EUG content. Particularly, the tensile strength of NBR/EUG composites improved from 4.4 to 13.0 MPa and the elongation at break increased from 409% to 689%, respectively, with increasing EUG content from 0% to 10%. Meanwhile, the incorporation of EUG obviously improved the sound absorption performances of various NBR/EUG composites. This study offered a new insight into the preparation of composite materials with controllable damping and sound absorption properties.

Author contributions

Writing – original draft preparation: Lin Su and Qi Wang; Writing – review & editing: Dexian Yin and Xiuying Zhao; Investigation, Ping Xiang, Xiaodong Ding and Li Liu; Methodology and Supervision: Xiuying Zhao; All authors have read and agreed to the published version of the manuscript.

Conflicts of interest

There are no conflicts to declare.

Acknowledgements

This research was funded by National Key Research and Development Program of China, grant number 2017YFB0306904.

References

1 S. A. Baghban, M. Khorasani and G. M. M. Sadeghi, *J. Polym. Res.*, 2020, **27**, 62.
2 A. Joy, S. Varughese, S. Shanmugam and P. Haridoss, *ACS Appl. Nano Mater.*, 2019, **2**, 736–743.
3 X. Q. Jia, S. Y. Li, H. J. Miu, T. Yang, K. Rao, D. Y. Wu, B. L. Cui, J. L. Ou and Z. C. Zhu, *Front. Chem.*, 2020, **8**, 683.
4 X. Wang, X. Chen, M. Song, Q. Wang, W. Zheng, H. Song, Z. Fan and A. Myat Thu, *Ind. Eng. Chem. Res.*, 2020, **59**, 11494–11504.
5 I. C. Tsimouri, S. Montibeller, L. Kern, P. J. Hine, R. Spolenak, A. A. Gusev and S. Danzi, *Compos. Sci. Technol.*, 2021, **208**, 108744.
6 C. Liu, J. Fan and Y. Chen, *Polym. Test.*, 2019, **79**, 106003.
7 F. Zhang, M. Guo, K. Xu, G. He, H. Wu and S. Guo, *Compos. Sci. Technol.*, 2014, **101**, 167–172.
8 C. Qu, S. Li, Y. Zhang, T. Wang, Q. Wang and S. Chen, *Tribol. Int.*, 2021, **163**, 107150.
9 T. Li, S. Chen, S. Wan, S. Cai and X. He, *Polym. Compos.*, 2020, **41**, 1867–1877.
10 N. Ning, X. Li, H. Tian, Y. Hua, H. Zuo, P. Yao, L. Zhang, Y. Wu, G.-H. Hu and M. Tian, *RSC Adv.*, 2017, **7**, 5451–5458.
11 L. Xia, Y. Wang, Z. Ma, A. Du, G. Qiu and Z. Xin, *Polym. Adv. Technol.*, 2017, **28**, 94–101.
12 G. Liu, X. Zhang, T. Zhang, J. Zhang, P. Zhang and W. Wang, *Polym. Test.*, 2017, **63**, 582–586.
13 X. Wei, P. Peng, F. Peng and J. Dong, *J. Agric. Food Chem.*, 2021, **69**, 3797–3821.
14 Y. Dong, D. Yin, L. Deng, R. Cao, S. Hu, X. Zhao and L. Liu, *Materials*, 2021, **14**, 7487.
15 R. Cao, L. Deng, Z. Feng, X. Zhao, X. Li and L. Zhang, *Polymer*, 2021, **213**, 123292.
16 H. Kang, L. Yao, Y. Li, X. Hu, F. Yang, Q. Fang and L. Zhang, *J. Appl. Polym. Sci.*, 2018, **135**, 46017.
17 Q. Fang, X. Jin, F. Yang, C. Ma, Y. Gao and N. Wang, *Polym. Bull.*, 2015, **73**, 357–367.
18 M. Dong, T. Zhang, J. Zhang, G. Hou, M. Yu and L. Liu, *Polym. Test.*, 2020, **87**, 106539.
19 X. Zong, S. Wang, N. Li, H. Li, X. Zhang and A. He, *Polymer*, 2021, **213**, 123325.
20 J. Zhang, Z. Xue and R. Yan, *Chin. J. Polym. Sci.*, 2010, **29**, 157–163.
21 J. Zhang and Z. Xue, *Polym. Bull.*, 2011, **67**, 511–525.
22 Sarina, J. Zhang and L. Zhang, *Polym. Bull.*, 2012, **68**, 2021–2032.
23 Q. Sun, X. Zhao, D. Wang, J. Dong, D. She and P. Peng, *Carbohydr. Polym.*, 2018, **181**, 825–832.
24 X. Qi, F. Xie, J. Zhang, L. Zhang and D. Yue, *RSC Adv.*, 2019, **9**, 42367–42374.
25 H. Nie, H. Ren, X. Han and A. He, *Polym. Test.*, 2019, **80**, 106120.
26 K. Yao, H. Nie, Y. Liang, D. Qiu and A. He, *Polymer*, 2015, **80**, 259–264.
27 Y. Wu, K. Yao, H. Nie and A. He, *Polymer*, 2018, **153**, 271–276.
28 J. Zhang and Z. Xue, *Polym. Test.*, 2011, **30**, 753–759.
29 D. Yin, J. Mi, H. Zhou, X. Wang and K. Yu, *J. Appl. Polym. Sci.*, 2020, **137**, 48850.
30 D. Yin, J. Mi, H. Zhou, X. Wang and H. Tian, *Carbohydr. Polym.*, 2020, **247**, 116708.
31 K. Shi, G. Jin, R. Liu, T. Ye and Y. Xue, *Results Phys.*, 2019, **12**, 132–142.
32 G. Cheng, D. HE and G. Shu, *Colloids Surf., A*, 2001, **179**, 191–194.
33 I. I. Kabir, Y. Fu, N. De Souza, J. C. Baena, A. C. Y. Yuen, W. Yang, J. Mata, Z. Peng and G. H. Yeoh, *J. Mater. Sci.*, 2020, **55**, 5048–5063.

© 2022 The Author(s). Published by the Royal Society of Chemistry